IRS-Aided Energy Efficient UAV Communication

Hyesang Cho
Korea Advanced Institute of Science and Technology
Junil Choi (junil@kaist.ac.kr)
Korea Advanced Institute of Science and Technology https://orcid.org/0000-0002-9862-9020

Research Article

Keywords: UAV communication, intelligent re ecting surface, energy consumption minimization, successive convex approximation

Posted Date: March 11th, 2022

DOI: https://doi.org/10.21203/rs.3.rs-1410830/v1

RESEARCH

IRS-Aided Energy Efficient UAV Communication

Hyesang Cho and Junil Choi*

Abstract

Unmanned aerial vehicle (UAV) communication systems are in active study due to its various applications. However, UAV communication systems suffer from energy consumption, which limits the flying time of UAVs. In this paper, we propose several UAV energy consumption minimization techniques through the aid of multiple intelligent reflecting surfaces (IRSs). In specific, we introduce a tractable model to effectively capture the characteristics of multiple IRSs and multiple user equipments (UEs). Then, we derive a closed form expression for the UE achievable rate, resulting in tractable optimization problems. Accordingly, we effectively solve the optimization problems by adopting the successive convex approximation technique. To compensate for the high complexity of the optimization problems, we propose a low complexity algorithm that has marginal performance loss. In the numerical results, we show that the proposed algorithms can save UAV energy consumption significantly compared to the benchmarks, justifying that exploiting the IRSs is indeed favorable to UAV energy consumption minimization.

Keywords: UAV communication, intelligent reflecting surface, energy consumption minimization, successive convex approximation

1 Introduction

Unmanned aerial vehicle (UAV) technology has steadily gained attention over time due to its attractive characteristics. By exploiting its mobility, the UAV can be used for various scenarios such as hazardous environments, dense urban cities, and military communications [1–8]. Accordingly, extensive research on UAV technology has been done, adopting the UAV for wireless communication as a mobile base station (BS) or a relay [9–12]. Unlike conventional ground nodes, the UAV can enjoy favorable channel conditions and avoid blockage via their high altitude.

Even with their potential, UAV communication systems have their limitations such as energy consumption [13]. While traditional devices replenish energy from a dedicated source, it is improbable for the UAV to replenish energy due to its wireless feature. Also, due to its hovering characteristic, the UAV has additional power consumption, which is usually orders of magnitude larger than communication power [14]. To address this issue, there have been works to maximize the energy efficiency of UAV communication systems. Especially, [15] minimized the energy consumption of a rotary-wing UAV communication system with a specific data constraint through jointly optimizing the UAV trajectory, velocity, and communication time.

Another novel technology that is gaining tremendous highlight is intelligent reflecting surfaces (IRSs) [16–18]. An IRS is a planar surface consisting of multiple passive elements, where each element has the ability to independently shift the phase of the electromagnetic waves impinging on itself [19–22]. By thoroughly adjusting the phase controller, the IRS can enhance the signal gain for a desired location, resulting in a virtual line-of-sight (LoS) path. Therefore, the IRS can function as a controllable relay with minimal power consumption.

Recently, there have been many attempts to combine UAV communication systems with IRSs, which can be divided into two large categories [23–26]. In the first category, the UAV itself is equipped with the IRS. In particular, [27] analyzed the outage probability, ergodic capacity, and energy efficiency of wireless communication systems supported by the IRS equipped UAV. In the second category, the UAV communication system is assisted through terrestrial IRSs. In [26], the secrecy rate was maximized by optimizing the IRS phase shifts, trajectory, and power for the UAV communication system. The work in [28] analyzed the coverage increase of a dual-hop relay system using the IRS and UAV. The multi-UAV non-orthogonal multi-

*Correspondence: junil@kaist.ac.kr
School of Electrical Engineering, Korea Advanced Institute of Science and Technology, Daejeon, Korea
Full list of author information is available at the end of the article
†This paper will be presented in part at the IEEE Wireless Communications and Networking Conference Workshops, 2022.

ple access system assisted with an IRS was considered in [29].

In addition, there have been some researches to increase the energy efficiency of the systems. In [30], the resource allocation for a power-efficient IRS-aided UAV system was studied. However, the UAV has to select between the IRS reflected path and the direct path, unable to simultaneously exploit the two paths. In [23], the trajectory was optimized to maximize the average achievable rate for a single user single IRS UAV system. The proposed method, however, is strictly restricted to the single IRS case, unable to generalize to a multiple IRS scenario. Finally, [31] maximized the reception power in a given time constraint using multiple IRSs by optimizing the phase shifts, transmit beamformer, and UAV trajectory. While [31] discussed a multiple IRS scenario, it did not reveal the tradeoff between the reception power and UAV flight power, e.g., the UAV may consume excess flight power to maximize the UE reception power. In addition, all these works assumed partially LoS channels, and did not exploit the intuitive benefit of the highly located IRSs, i.e., the highly located IRSs have the advantage of gaining the LoS paths. Accordingly, this tempts us to explore UAV energy consumption minimization in a more realistic multiple terrestrial IRS scenario.

In this paper, we propose several UAV energy consumption minimization algorithms with a specific data constraint for the most general case of multiple IRSs and multiple user equipments (UEs). The main insight is that by increasing the received data rate at the UEs through the IRSs, we can reduce the flight time, thus, reduce the UAV energy consumption. In specific, we first expand the probabilistic LoS model to capture the advantage of deploying IRSs on tall buildings [32]. To the best of our knowledge, this is the first work to consider the popular probabilistic LoS channel model for UAV scenarios in IRS assisted environments. By utilizing the new system model, we derive the optimal IRS phase shifts and develop a closed form of the UE achievable rate. We then formulate the optimization problem that jointly optimizes the trajectory, flight speed, and communication time of the UAV. Afterwards, we transform the optimization problem into tractable forms exploiting slack variables and effectively solve them through the well known successive convex approximation (SCA) technique [25]. Finally, we propose a low complexity algorithm that tries to follow the behavior of a specific optimization problem solution, resulting in comparable performance with respect to the jointly optimized results.

The rest of paper is organized as follows. Section 2 describes the power consumption model of the rotary-wing UAV and the channel model of the system. In Section 3, we derive the closed form expression of the UE achievable rate and formulate the UAV energy consumption minimization problem. In Section 4, we introduce several algorithms to effectively solve the joint optimization problem. Section 5 shows the simulation results of the proposed techniques with benchmark schemes. Finally, Section 6 concludes the paper.

Notation: Lower and upper boldface letters represent column vectors and matrices. $\mathbf{A}^*$ and $\mathbf{A}^{\mathrm{H}}$ denotes the conjugate, and conjugate transpose of the matrix $\mathbf{A}$. $\mathrm{diag}(\mathbf{a})$ returns the diagonal matrix with $\mathbf{a}$ on its diagonal. $\{\mathbf{a}\}^b$ represents the set of length b vectors with each element from $\mathbf{a}$. $\mathbb{C}^{m\times n}$ and $\mathbb{R}^{m\times n}$ represent the set of all $m \times n$ complex and real matrices. $|\cdot|$ denotes the amplitude of the scalar, and $\|\cdot\|$ represents the ℓ_2-norm of the vector. $\mathcal{O}$ denotes the Big-O notation. $\mathbf{0}_m$ is used for the $m \times 1$ all zero vector, and $\mathbf{I}_m$ denotes the $m \times m$ identity matrix. $\mathcal{CN}(\mathbf{m}, \mathbf{\Sigma})$ denotes the circularly symmetric complex Gaussian distribution with mean $\mathbf{m}$ and variance $\mathbf{\Sigma}$.

2 System Model

In this paper, we consider a wireless communication system where a rotary-wing UAV supports multiple UEs with the aid of multiple IRSs as in Fig. 1. We assume a single antenna UAV, K single antenna UEs, and W IRSs, with the w-th IRS having M_w IRS elements. The UAV freely hovers around the horizontal plane, where the horizontal location at time t is denoted as $\mathbf{q}(t) \in \mathbb{R}^{2\times 1}$, and the altitude is fixed as $H_{\mathrm{A}} \in \mathbb{R}$. Since the IRSs are typically located to gain a better LoS condition, we assume that the IRSs are installed on the outer walls of tall buildings, thus, having more height than the UEs. We assume that the w-th IRS is fixed with the horizontal location $\mathbf{q}_{\mathrm{I}_w} \in \mathbb{R}^{2\times 1}$ and height $H_{\mathrm{I}_w} \in \mathbb{R}$. Also, we assume that the UEs are located without mobility with the horizontal location and height of the k-th UE denoted as $\mathbf{q}_{\mathrm{U}_k} \in \mathbb{R}^{2\times 1}$ and $H_{\mathrm{U}_k} \in \mathbb{R}$, respectively.

2.1 UAV Power Consumption Model

Since we assumed to use the rotary-wing UAV, we adopt the popular rotary-wing UAV flight power consumption model from [15, 30], which is given as

$$P(V) = P_0\left(1+\frac{3V^2}{U_{\mathrm{tip}}^2}\right) + P_i\left(\sqrt{1+\frac{V^4}{4v_0^4}}-\frac{V^2}{2v_0^2}\right)^{1/2} + \frac{1}{2}d_0\rho s A_{\mathrm{p}} V^3, \tag{1}$$

where V is the UAV speed and the other variables are listed in Table 1. The total energy consumption of the

Table 1: UAV flight power consumption variables [15].

Variable	Description	Value
P_0	Blade profile power	79.86
P_i	Induced power	88.63
U_{tip}	Rotor blade tip speed	120
v_0	Rotor induced velocity	4.03
d_0	Fuselage drage ratio	0.6
ρ	Air density	1.225
s	Motor solidity	0.05
A_{p}	Rotor disc area	0.503

UAV can be expressed as

$$E_{\text{tot}} = \tau P_c + \int_0^T P\left(V(t)\right) dt, \tag{2}$$

where τ is the communication time and T is the total flight time of the UAV. We observe that the power consumption is dependent on the UAV speed, and that the model itself is quite complicated. This leads us to believe that the UAV speed should also be jointly optimized to effectively minimize the UAV power consumption. Also, we can confirm that while the power consumption for communication usually has the magnitude of 1 W or smaller, the power consumption from UAV hovering has the magnitude of 100 W. Thus, it is obvious that we must consider the UAV flight power to successively achieve energy efficient UAV communication systems.

2.2 Channel Model

To capture the characteristic of the UAV, we adopt the well-known probabilistic LoS model [32], which models the LoS path existence probability as a variable dependent on the elevation angle between a node and a UAV. The LoS path existence probability is given as [32]

$$p_i(t) = \frac{1}{1 + a_i \exp\left(-b_i\left(\theta_i(t) - a_i\right)\right)}, i \in \{\mathrm{I}_w, \mathrm{U}_k\}, \tag{3}$$

where $p_{\mathrm{I}_w}(t)$ and $p_{\mathrm{U}_k}(t)$ denote the LoS path existence probabilities between the UAV to the w-th IRS and UAV to the k-th UE, respectively. The variables a_i and b_i are the design parameters dependent on the environment, and $\theta_i(t)$ is the elevation angle, which can be expressed as $\theta_i(t) = \frac{180}{\pi} \sin^{-1}\left(\frac{H_{\text{A}} - H_i}{d_i(t)}\right)$. Note that, due to the height of the installed IRSs, we consider the design parameters a_i and b_i as variables. Defined in [32], the design parameters are dependent on the average building height and building density with respect to the ground. Therefore, by taking the height of the installed IRSs on buildings as the new effective ground, the average building height and density which the IRSs see will decrease, resulting in a relatively rural environment with respect to the original environment. This new consideration can effectively capture the fact that highly located IRSs are favorable in obtaining the LoS path. Note that, the design parameters a_i and b_i can adapt to each IRS or UE, thus, this model can effectively consider the different heights of the IRSs or even consider the highly located UEs.

For the channels associated with the UAV, the UAV to the w-th IRS channel and the UAV to the k-th UE channel are denoted as $\mathbf{h}_{\mathrm{I}_w}(t) \in \mathbb{C}^{M_w \times 1}$ and $h_{\mathrm{U}_k}(t) \in \mathbb{C}$, respectively. By taking the probabilistic LoS model into account, the effective channels can be expressed as

$$\mathbf{h}_{\mathrm{I}_w}(t) = \begin{cases} \mathbf{h}_{\mathrm{I}_w,\mathrm{Ri}}(t), \text{Probability } p_{\mathrm{I}_w}(t), \\ \nu_{\mathrm{I}_w} \mathbf{h}_{\mathrm{I}_w,\mathrm{Ra}}(t), \text{Probability } 1 - p_{\mathrm{I}_w}(t), \end{cases} \tag{4}$$

$$h_{\mathrm{U}_k}(t) = \begin{cases} h_{\mathrm{U}_k,\mathrm{Ri}}(t), \text{Probability } p_{\mathrm{U}_k}(t), \\ \nu_{\mathrm{U}_k} h_{\mathrm{U}_k,\mathrm{Ra}}(t), \text{Probability } 1 - p_{\mathrm{U}_k}(t), \end{cases} \tag{5}$$

where $\nu_i < 1,\ i \in \{\mathrm{I}_w, \mathrm{U}_k\}$, is the attenuation factor to consider the relatively small power of the non-LoS path, and the effective channels are given as

$$\mathbf{h}_{\mathrm{I}_w,\mathrm{Ri}}(t) = L_{\mathrm{I}_w}(t) \mathbf{g}_{\mathrm{I}_w,\mathrm{Ri}}(t), \tag{6}$$

$$\mathbf{h}_{\mathrm{I}_w,\mathrm{Ra}}(t) = L_{\mathrm{I}_w}(t) \mathbf{g}_{\mathrm{I}_w,\mathrm{Ra}}(t), \tag{7}$$

$$h_{\mathrm{U}_k,\mathrm{Ri}}(t) = L_{\mathrm{U}_k}(t) g_{\mathrm{U}_k,\mathrm{Ri}}(t), \tag{8}$$

$$h_{\mathrm{U}_k,\mathrm{Ra}}(t) = L_{\mathrm{U}_k}(t) g_{\mathrm{U}_k,\mathrm{Ra}}(t), \tag{9}$$

where $L_i(t) = \sqrt{\beta_0 d_i^{-\alpha_i}(t)}$ is the large-scale fading factor with β_0 as the pathloss at a reference distance of 1 m, $d_i(t)$ as the distance between nodes, and α_i as the pathloss exponent. The variables $\mathbf{g}_i(t)$ and $g_i(t)$ are the small-scale fading channels given as

$$\begin{aligned} \mathbf{g}_{\mathrm{I}_w,\mathrm{Ri}}(t) = &\sqrt{\frac{\kappa_{\mathrm{I}_w}}{\kappa_{\mathrm{I}_w} + 1}} \mathbf{e}_{\mathrm{I}_w}(t) \\ &+ \sqrt{\frac{1}{\kappa_{\mathrm{I}_w} + 1}} \mathbf{g}_{\mathrm{I}_w,\mathrm{Ra}}(t), \end{aligned} \tag{10}$$

$$\begin{aligned} g_{\mathrm{U}_k,\mathrm{Ri}}(t) = &\sqrt{\frac{\kappa_{\mathrm{U}_k}}{\kappa_{\mathrm{U}_k} + 1}} e^{j\psi_{\mathrm{U}_k}}(t) \\ &+ \sqrt{\frac{1}{\kappa_{\mathrm{U}_k} + 1}} g_{\mathrm{U}_k,\mathrm{Ra}}(t). \end{aligned} \tag{11}$$

The vector $\mathbf{e}_{\mathrm{I}_w} = \left[\exp(j\psi_{\mathrm{I}_w,1}), ..., \exp(j\psi_{\mathrm{I}_w,M_w})\right]^{\mathrm{T}}$ and scalar $e^{j\psi_{\mathrm{U}_k}}$ denote the LoS paths with $\psi_{\mathrm{I}_w,m}$ and ψ_{U_k} representing the phases of the channels between the

UAV to the m-th IRS element of the w-th IRS and the UAV to the k-th UE, respectively. Also, the channels $\mathbf{g}_{\mathrm{I}_w,\mathrm{Ri}}(t)$ and $g_{\mathrm{U}_k,\mathrm{Ri}}(t)$ follow the Rician distribution with K-factors as κ_{I_w} and κ_{U_k}, respectively, and $\mathbf{g}_{\mathrm{I}_w,\mathrm{Ra}}(t) \sim \mathcal{CN}(\mathbf{0}_{M_w}, \mathbf{I}_{M_w})$ and $g_{\mathrm{U}_k,\mathrm{Ra}}(t) \sim \mathcal{CN}(0,1)$ are the non-LoS components. In result, the air-to-ground channels follow the Rician distribution when the LoS paths exist, and follow the Rayleigh distribution in the opposite case. We assume that the w-th IRS to the k-th UE channel $\mathbf{h}_{wk}(t) \in \mathbb{C}^{M_w \times 1}$ is formulated similarly to $\mathbf{h}_{\mathrm{I}_w,\mathrm{Ri}}(t)$ with the K-factor as κ_{wk}, which is omitted due to redundancy.

Overall, the channel for the k-th UE is given as

$$\bar{h}_k(t) = \sum_{w=1}^{W} \left(\mathbf{h}_{wk}^{\mathrm{H}}(t)\mathbf{\Phi}_w(t)\mathbf{h}_{\mathrm{I}_w}(t)\right) + h_{\mathrm{U}_k}(t), \quad (12)$$

where $\mathbf{\Phi}_w$ is the phase control matrix of the w-th IRS. The phase control matrix can be represented as $\mathbf{\Phi}_w = \mathrm{diag}(\boldsymbol{\phi}_w)$, with $\boldsymbol{\phi}_w = [\exp(j\phi_{w,1}), ..., \exp(j\phi_{w,M_w})]^{\mathrm{T}}$, thus, the m-th IRS element of the w-th IRS will shift the phase of the impinging signal with the factor $\phi_{w,m}$. We remark that the signals reflecting on multiple IRSs are neglected due to the harsh propagation of multiple propagation losses.

In this paper, we adopt the time-division multiple access (TDMA) technique at the UAV to serve the K UEs to efficiently prevent inter-user interference [6–8, 15, 30]. Thus, when the k-th UE is served, the received signal is given as

$$y_k(t) = \bar{h}_k(t)P_c\xi_k(t) + n_k(t), \quad (13)$$

where $\xi_k(t) \sim \mathcal{CN}(0,1)$ is the transmit signal for the k-th UE, $n_k(t) \sim \mathcal{CN}(0,\sigma^2)$ is the noise of the k-th UE with the noise spectral density σ^2, and P_c is the transmit power of the UAV. Then, the achievable rate for the k-th UE can be denoted as

$$\bar{R}_k(t) = B\log_2\left(1 + \frac{P_c|\bar{h}_k(t)|^2}{B\sigma^2}\right), \quad (14)$$

where B is the bandwidth.

3 Problem formulation

In this section, we formulate the overall UAV energy consumption minimization problem. Specifically, we first derive the closed form expression for the IRS phase shifts and the achievable rate through various mathematical techniques. Thereafter, we define the UAV energy consumption minimization problem that jointly optimizes the UAV trajectory, speed, and flight time.

3.1 Achievable Rate Derivation

To minimize the UAV energy consumption while sufficing a specific data constraint, it is trivial to operate the IRS phase shifts to maximize the achievable rate. While deriving the IRS phase shifts jointly considering multiple UEs may be cumbersome and even untractable, due to the TDMA technique, we can effectively consider a single UE at a given time instance. Without loss of generality, we assume to serve the k-th UE. Note that, we need the instantaneous channel state information (CSI) to correctly adjust the IRS phase shifts. To focus on the achievable theoretical performance, we assume to have perfect CSI as in [23, 24, 31]. While channel estimation of IRS and UAV systems are promising areas of research, we believe that it is out of the scope of this paper, leaving it for future work.

Since maximizing the achievable rate is equivalent to maximizing the channel gain, we derive the optimal IRS phase shifts maximizing the channel norm. The channel norm for the k-th UE is given as

$$\begin{aligned}|\bar{h}_k(t)| &= |h_{\mathrm{U}_k}(t) + \sum_{w=1}^{W}\left(\mathbf{h}_{wk}^{\mathrm{H}}(t)\mathbf{\Phi}_w(t)\mathbf{h}_{\mathrm{I}_w}(t)\right)| \\ &= |h_{\mathrm{U}_k}(t) + \sum_{w=1}^{W}\sum_{m=1}^{M_w} h_{\mathrm{I}_w,m}(t) \\ &\quad \times h_{wk,m}(t)e^{j\phi_{w,m}}|. \end{aligned} \quad (15)$$

Using the Triangle inequality, the norm can be bounded as

$$|\bar{h}_k(t)| \le |h_{\mathrm{U}_k}(t)| + \sum_{w=1}^{W}\sum_{m=1}^{M_w}|h_{\mathrm{I}_w,m}(t)||h_{wk,m}(t)|, \quad (16)$$

where the equality holds when the UAV-IRS-UE channels are coherently combined with the UAV-UE channel. In result, to gain the upper bound, the reflection coefficient of the m-th IRS element of the w-th IRS is given as

$$\phi_{w,m}(t) = \angle\left(h_{\mathrm{U}_k}(t)\right) - \angle\left(h_{\mathrm{I}_w,m}(t)\right) \quad (17)$$

$$+ \angle\left(h_{wk,m}(t)\right), \quad (18)$$

where $h_{\mathrm{I}_w,m}(t)$ and $h_{wk,m}(t)$ denote the m-th element of the channel vectors $\mathbf{h}_{\mathrm{I}_w}(t)$ and $\mathbf{h}_{wk}(t)$, respectively. Thus, by maximizing the channel gain, the IRS phase shifts will optimally maximize the achievable rate for the k-th UE.

To gain tractability, we adopt two frequently used assumptions as in [15]. First, since predicting the future channel values to design the trajectory is improbable, we use the expected achievable rate instead of the

instantaneous achievable rate. Note that, this might seem as if perfect CSI is unnecessary. However, to obtain the expected achievable rate, we need the IRSs to constantly adapt to the instantaneous channels for the coherent combination, thus, the assumption of perfect CSI is still necessary. Second, due to the involved form of (3), we assume that the LoS path existence probabilities are constant with respect to time, e.g., fix the probabilities with the average elevation angles. Nevertheless, the simplified model still captures the advantage of the highly located IRSs.

To effectively express the probabilistic LoS model, we define a state variable as

$$\mathbf{s}_k = \left[s_{\mathrm{U}_k}, s_{\mathrm{I}_1}, ..., s_{\mathrm{I}_W}\right]^{\mathrm{T}},\ s_i \in \{0,1\}, \tag{19}$$

for $i \in \{\mathrm{U}_k, \mathrm{I}_w\}$, where s_{U_k} and s_{I_w} denote the states of the UAV-(k-th UE) path and UAV-(w-th IRS) path, respectively, and $s_i = 1$ represents the LoS path existence of the selected path. With this variable, we can upper bound the expected achievable rate of the k-th UE using the Jensen's inequality as

$$\begin{aligned}
&\mathbb{E}\left[\bar{R}_k(t)\right] \\
&= \sum_{\mathbf{s}_k \in \mathcal{S}} \prod_i p_i^{s_i} \left(1-p_i\right)^{1-s_i} \\
&\times \mathbb{E}\left[B \log_2\left(1 + \frac{P_c |\bar{h}_{\mathbf{s}_k}(t)|^2}{B\sigma^2}\right)\right] \\
&\leq \sum_{\mathbf{s}_k \in \mathcal{S}} \prod_i p_i^{s_i} \left(1-p_i\right)^{1-s_i} \\
&\times B \log_2\left(1 + \frac{P_c \mathbb{E}\left[|\bar{h}_{\mathbf{s}_k}(t)|^2\right]}{B\sigma^2}\right) \\
&= \hat{R}_k(t),\ i \in \{\mathrm{U}_k, \mathrm{I}_w\},
\end{aligned} \tag{20, 21}$$

where $\mathcal{S} = \{0,1\}^{W+1}$, and $\bar{h}_{\mathbf{s}_k}(t)$ is the overall channel between the UAV and the k-th UE considering the state variable. We observe that the closed form of (21) can be derived by computing $\mathbb{E}\left[|\bar{h}_{\mathbf{s}_k}(t)|^2\right]$. However, $\mathbb{E}\left[|\bar{h}_{\mathbf{s}_k}(t)|^2\right]$ is difficult to derive due to the joint consideration of the UAV-UE channel and the UAV-IRS-UE channel.

To compute the expected channel gain, we first assume that the IRS phases are coherently combining the UAV-UE channel and the UAV-IRS-UE channel as in (17). In result, the overall channel norm for the k-th UE is given as

$$\begin{aligned}
|\bar{h}_{\mathbf{s}_k}(t)| &= s_{\mathrm{U}_k} |h_{\mathrm{U}_k,\mathrm{Ri}}(t)| + (1 - s_{\mathrm{U}_k}) |\nu_{\mathrm{U}_k} h_{\mathrm{U}_k,\mathrm{Ra}}(t)| \\
&+ \sum_{w=1}^{W} s_{\mathrm{I}_w} \sum_{m=1}^{M_w} |h_{\mathrm{I}_w,\mathrm{Ri},m}(t)||h_{wk,m}(t)| \\
&+ \sum_{w=1}^{W} (1 - s_{\mathrm{I}_w}) \\
&\times \sum_{m=1}^{M_w} |\nu_{\mathrm{I}_w} h_{\mathrm{I}_w,\mathrm{Ra},m}(t)||h_{wk,m}(t)|.
\end{aligned} \tag{22}$$

We note that, the effect of $\nu_i,\ i \in \{\mathrm{I}_w, \mathrm{U}_k\}$ is minimal due to the small channel gains of non-LoS paths, but results in cumbersome computations. Thus, from hereafter, we take $\nu_i = 0$ for equational conciseness[1]. By defining $C_0(t) = s_{\mathrm{U}_k} |h_{\mathrm{U}_k}(t)|$ and $C_w(t) = s_{\mathrm{I}_w} \sum_{m=1}^{M_w} |h_{\mathrm{I}_w,m}(t)||h_{wk,m}(t)|$ for $w \in \{1,2,...,W\}$, we can expand the expected channel gain as

$$\begin{aligned}
\mathbb{E}\left[|\bar{h}_{\mathbf{s}_k}(t)|^2\right] &= \sum_{i=0}^{W} \mathbb{E}\left[C_i^2(t)\right] \\
&+ \sum_{i=0}^{W} \sum_{j \neq i}^{W} \mathbb{E}\left[C_i(t)\right] \mathbb{E}\left[C_j(t)\right],
\end{aligned} \tag{23}$$

where the multiplication between $C_i(t)$ and $C_j(t), i \neq j$ can be separated due to independence. Note that $C_w(t)$ is the sum of M_w i.i.d. variables. Considering that the number of IRS elements M_w is predicted to be installed in large quantities, we employ the central limit theorem and assume that $C_w(t)$ follows the Gaussian distribution and that $C_w^2(t)$ follows the non-central Chi-squared distribution. Overall, (21) can be shown as

$$\hat{R}_k(t) = \sum_{\mathbf{s}_k \in \mathcal{S}} \prod_i p_i^{s_i} \left(1-p_i\right)^{1-s_i} \log_2\left(1 + \hat{\gamma}_{\mathbf{s}_k}(t)\right), \tag{24}$$

with the overall signal-to-noise ratio (SNR) in the closed form expression as

$$\begin{aligned}
\hat{\gamma}_{\mathbf{s}_k}(t) &= \sum_i s_i \gamma_i^2 d_i^{-\alpha_i}(t) \\
&+ \sum_i \sum_{j \neq i} s_i s_j \gamma_i' \gamma_j' d_i^{-\alpha_i/2}(t) d_j^{-\alpha_j/2}(t),
\end{aligned} \tag{25}$$

[1] Although we take $\nu_i = 0$ for conciseness, the achievable rate for the general $\nu_i \neq 1$ case can be similarly derived by exploiting the Rayleigh distribution of the non-LoS paths.

for $i \in \{\mathrm{U}_k, \mathrm{I}_1, ..., \mathrm{I}_W\}$, where we substitute s_i^2 with s_i since $s_i^2 = s_i$, and the variables γ_i and γ_i' are defined as

$$\gamma_{\mathrm{U}_k} = \sqrt{\frac{\beta_0 P_c}{B\sigma^2}}, \tag{26}$$

$$\gamma'_{\mathrm{U}_k} = \sqrt{\frac{\beta_0 P_c}{B\sigma^2}}\mu\left(\kappa_{\mathrm{U}_k}\right), \tag{27}$$

$$\gamma_{\mathrm{I}_w} = \sqrt{\frac{\beta_0^2 P_c}{d_{wk}^{\alpha_{wk}} B\sigma^2}}\sqrt{\mu_{\mathrm{I}_w}^2 + 1}, \tag{28}$$

$$\gamma'_{\mathrm{I}_w} = \sqrt{\frac{\beta_0^2 P_c}{d_{wk}^{\alpha_{wk}} B\sigma^2}}\mu_{\mathrm{I}_w}, \tag{29}$$

where $\mu\left(\kappa_i\right)$ denotes the mean of the Rician distribution with the K-factor as κ_i, and $\mu_{\mathrm{I}_w} = M_w \mu\left(\kappa_{\mathrm{I}_w}\right) \times \mu\left(\kappa_{wk}\right)$. Note that the channel state with no LoS paths are zero due to the assumption $\nu_i = 0$, where the case $\nu_i \neq 0$ gives only constant value differences in (26)-(29).

In Fig. 2, we plot the approximated achievable rate, simulated achievable rate, and the achievable rate bound in [15] for the single IRS single UE case with the same parameters in Section 5. We observe that the approximated achievable rate is tightly bounded with the simulated achievable rate. Moreover, by introducing the state variable, the figure clearly shows that the approximated achievable rate is much tighter than the bound from [15]. Thus, hereinafter, we consider $\hat{R}_k(t)$ as the achievable rate of the UE.

3.2 Optimization Problem Formulation

In this subsection, we formulate the UAV energy consumption minimization problem. Since optimizing with respect to continuous time will result in an infinite number of variables, we adopt the path discretization technique as in [15], where the trajectory is discretized into small segments. By segmenting the trajectory into N pieces, the UAV energy consumption minimization problem can be formulated as

$$\text{(P1)}: \min_{\mathbf{T},\boldsymbol{\tau},\mathbf{q}} \sum_{n=1}^{N}\left\{T_n P(V_n) + \sum_{k=1}^{K}\tau_{nk}P_c\right\}$$

$$\text{s.t. } \mathbf{q}[1] = \mathbf{q}_0,\ \mathbf{q}[N+1] = \mathbf{q}_{\mathrm{F}}, \tag{P1-a}$$

$$\sum_{k=1}^{K}\tau_{nk} \le T_n,\ \tau_{nk} \ge 0, \tag{P1-b}$$

$$\Delta_n \le \min\{\Delta_{\max}, V_{\max}T_n\}, \tag{P1-c}$$

$$\sum_{n=1}^{N}\tau_{nk}\hat{R}_{nk} \ge Q_k, \tag{P1-d}$$

where T_n, V_n, and $\mathbf{q}\left[n\right]$ are the UAV flight time, UAV speed, and UAV horizontal location at the n-th segment, respectively. Also, τ_{nk} and $\hat{R}_{nk}$ are the UAV transmission time and the achievable rate for the k-th UE at the n-th segment, respectively. Note that, $\hat{R}_{nk}$ can be obtained simply by replacing t with n in (24) and (25). We assume the UAV has fixed initial and final locations $\mathbf{q}_0$ and $\mathbf{q}_{\mathrm{F}}$, respectively, as in (P1-a). The sum of the UE transmission times are trivially bounded by the flight time as in (P1-b). One characteristic of the path discretization technique is it assumes that the channels are constants within a segment. To uphold this assumption, for the segment length $\Delta_n = \|\mathbf{q}[n+1] - \mathbf{q}[n]\|$, we bound the length with $\min\{\Delta_{\max}, V_{\max}T_n\}$, where $\Delta_{\max}$ is the maximum length of a segment to conserve this assumption, and $V_{\max}$ is the maximum speed of the UAV. Since the channel is assumed to be a constant within a segment, the achievable rate is also a constant. Thus, $\tau_{nk}\hat{R}_{nk}$ is the transmitted data within a segment, and we assume the k-th UE has a fixed data constraint Q_k as in (P1-d).

While (P1) seems to have a similar form as [15], it is not possible to directly apply the framework of [15] since the IRSs cause a complex achievable rate expression. Therefore, $\hat{R}_{nk}$ needs delicate and strong mathematical derivations to successfully boil down into the framework developed in [15], which will become clear in Section 4.

4 Proposed Algorithms

In this section, we solve the optimization problem (P1) through various approaches. Specifically, we propose two different cases to effectively solve (P1) with similar performance. In addition, we propose an algorithm to mimic the behavior of a specific optimization problem to achieve low UAV energy consumption with minimal complexity.

4.1 General IRS Usage Case

The most straightforward approach to exploit the multiple IRSs is to use all of them simultaneously, which is equal to problem (P1). We denote this approach as the general IRS usage case. Similar to (P4) in [15], we

transform (P1) into an equivalent problem as

$$\begin{aligned}(\text{P2}): \min_{\mathcal{V}} & \sum_{n=1}^{N}\sum_{k=1}^{K}\tau_{nk}P_c + P_0\left(T_n + \frac{\delta_b\Delta_n^2}{T_n}\right) \\ & + \delta_p\frac{\Delta_n^3}{T_n^2} + P_i y_n \\ \text{s.t. } & d_{\mathrm{I}_w,n} \le u_{nw},\ d_{\mathrm{U}_k,n} \le v_{nk}, && \text{(P2-a)} \\ & Q_k \le \sum_{n=1}^{N} A_{nk}^2, && \text{(P2-b)} \\ & \frac{A_{nk}^2}{\tau_{nk}} \le R_{nk}, && \text{(P2-c)} \\ & \frac{T_n^4}{y_n^2} \le y_n^2 + \frac{\Delta_n^2}{v_0^2}, && \text{(P2-d)} \\ & \text{(P1-a)}, \text{(P1-b)}, \text{(P1-c)},\end{aligned}$$

where $\delta_b = 3U_{\text{tip}}^{-2}$, $\delta_p = \frac{1}{2}d_0\rho s A_{\text{p}}$, and $\mathcal{V}$ is the set of variables $\mathcal{V} = \{\mathbf{A}, \mathbf{y}, \boldsymbol{\tau}, \mathbf{T}, \mathbf{q}, \mathbf{u}_w, \mathbf{v}_k\}$. The transformation with regard to slack variables A_{nk} and y_n, which are the (n,k)-th and n-th elements of $\mathbf{A}$ and $\mathbf{y}$, respectively, are equivalent as in [15], thus, we omit the transformation details. The slack variables u_{nw} and v_{nk} are the n-th elements of the vectors $\mathbf{u}_w$ and $\mathbf{v}_k$, where they upper bound the UAV-IRS distance and the UAV-UE distance, respectively, which are given as

$$d_{\mathrm{I}_w,n} = \|[\mathbf{q}^{\mathrm{T}}[n], H_{\mathrm{A}}] - [\mathbf{q}_{\mathrm{I}_w}^{\mathrm{T}}, H_{\mathrm{I}_w}]\|, \tag{30}$$

$$d_{\mathrm{U}_k,n} = \|[\mathbf{q}^{\mathrm{T}}[n], H_{\mathrm{A}}] - [\mathbf{q}_{\mathrm{U}_k}^{\mathrm{T}}, H_{\mathrm{U}_k}]\|. \tag{31}$$

Also, R_{nk} is the achievable rate with the slack variables u_{nw} and v_{nk} instead of $d_{\mathrm{I}_w,n}$ and $d_{\mathrm{U}_k,n}$, respectively, which can be expressed as

$$R_{nk} = \sum_{\mathbf{s}_k\in\mathcal{S}}\prod_i p_i^{s_i}(1-p_i)^{1-s_i}\log_2(1+\gamma_{\mathbf{s}_k,n}), \tag{32}$$

$$\begin{aligned}\gamma_{\mathbf{s}_k,n} = {} & s_{\mathrm{U}_k}\gamma_{\mathrm{U}_k}^2 v_{nk}^{-\alpha_{\mathrm{U}_k}} + \sum_{w=1}^{W} s_{\mathrm{I}_w}\gamma_{\mathrm{I}_w}^2 u_{nw}^{-\alpha_{\mathrm{I}_w}} \\ & + \sum_{w=1}^{W} 2s_{\mathrm{U}_k}s_{\mathrm{I}_w}\gamma'_{\mathrm{U}_k}\gamma'_{\mathrm{I}_w} v_{nk}^{-\alpha_{\mathrm{U}_k}/2} u_{nw}^{-\alpha_{\mathrm{I}_w}/2} \\ & + \sum_{w=1}^{W}\sum_{z\neq w}^{W} s_{\mathrm{I}_w}s_{\mathrm{I}_z}\gamma'_{\mathrm{I}_w}\gamma'_{\mathrm{I}_z} u_{nw}^{-\alpha_{\mathrm{I}_w}/2} u_{nz}^{-\alpha_{\mathrm{I}_z}/2}.\end{aligned} \tag{33}$$

Since $\gamma_{\mathbf{s}_k,n}$ is a decreasing function of variables $\{u_{nw}\}$ and v_{nk}, we observe that $R_{nk} \le \hat{R}_{nk}$. Therefore, if there is a solution where (P2-a) is not met with equality, the slack variables $\mathbf{u}_w$ and $\mathbf{v}_k$ will decrease to increase R_{nk}. In result, we see that (P2) is indeed equivalent to (P1). We observe that by considering the IRSs, the achievable rate has an involved form compared to the achievable rate with no IRSs, which makes the analysis difficult. To the best of our knowledge, this is the first paper to acknowledge the achievable rate for a general number of IRSs.

While the objective function is a convex function, the constraints (P2-b)-(P2-d) do not follow the standard convex optimization problem form. To resolve this issue, we adopt the well known SCA technique. By deriving a global bound of a constraint that meets specific conditions, the SCA technique iteratively solves the optimization problem and guarantees to converge to a Karush-Kuhn-Tucker (KKT) condition point [33]. One way to obtain the global lower bound satisfying the specific conditions is to apply the first-order Taylor expansion to a convex function on a local point. The right hand side of the constraints (P2-b) and (P2-d) have been shown to be convex in [15], while R_{nk} from (P2-c) needs to be analyzed. To do this, we state the following lemma.

Lemma 1 *For given non-negative constants $\epsilon_z, \zeta_z, \alpha_z$, $z \in \{1, 2, ..., Z\}$, the function given as*

$$f(u_1, ..., u_Z) = \log_2\left(h(u_1, ..., u_Z)\right), \tag{34}$$

with

$$\begin{aligned}h(u_1, ..., u_Z) = {} & 1 + \sum_{z=1}^{Z}\epsilon_z u_z^{-\alpha_z} \\ & + \sum_{z=1}^{Z}\sum_{i\neq z}^{Z}\zeta_z\zeta_i u_z^{-\alpha_z/2} u_i^{-\alpha_i/2}\end{aligned} \tag{35}$$

is convex with respect to $u_z > 0, z \in \{1, 2, ..., Z\}$ for any non-negative integer Z.

Proof The proof is given in Appendix A. □

Since p_i and $(1-p_i)$ are non-negative constants and $\log_2(1+\gamma_{\mathbf{s}_k,n})$ follows the form of $f(u_1, ..., u_Z)$, R_{nk} is a weighted linear sum of convex functions, thus, through Lemma 1, we confirm that R_{nk} is indeed a convex function. Due to the convexity of R_{nk}, we can successfully use the first-order Taylor expansion of R_{nk} as the lower bound.

Adopting the lower bound of the constraints (P2-b)-(P2-d), the overall optimization problem in the ℓ-th

Algorithm 1 Pseudo-code for the UAV energy consumption minimization algorithm

1: **Initialization:** Set $A_{nk}^{(0)}, y_n^{(0)}, \Delta_n^{(0)}, \mathbf{q}^{(0)}[n], u_{nw}^{(0)}, v_{nk}^{(0)}$, and $R_{nk}^{(0)}$. Let $\ell = 0$.
2: **repeat**
3: Set $\ell = \ell + 1$.
4: Solve the optimization problem (P3).
5: Update the solution of (P3) as $A_{nk}^{(\ell)}, y_n^{(\ell)}, \Delta_n^{(\ell)}$, $\mathbf{q}^{(\ell)}[n], u_{nw}^{(\ell)}, v_{nk}^{(\ell)}$, and $R_{nk}^{(\ell)}$.
6: **until** The UAV energy consumption E_{tot} decreases by a fraction below a predefined threshold.

iteration can be expressed as

$$\begin{aligned}(\text{P3}): \min_{\mathcal{V}} & \sum_{n=1}^{N}\sum_{k=1}^{K}\tau_{nk}P_c + P_0\left(T_n + \frac{\delta_b\Delta_n^2}{T_n}\right) \\ & + \delta_p\frac{\Delta_n^3}{T_n^2} + P_i y_n \\ \text{s.t. } & Q_k \le \sum_{n=1}^{N}\tilde{A}_{nk}^{(\ell)},\ \frac{A_{nk}^2}{\tau_{nk}} \le \tilde{R}_{nk}^{(\ell)}, \qquad \text{(P3-a)} \\ & \frac{T_n^4}{y_n^2} \le \tilde{Y}_n^{(\ell)}, \qquad \text{(P3-b)} \\ & \text{(P1-a), (P1-b), (P1-c), (P2-a),}\end{aligned}$$

where the lower bound functions are defined as

$$\tilde{A}_{nk}^{(\ell)} = A_{nk}^{(\ell)2} + 2A_{nk}^{(\ell)}\left(A_{nk} - A_{nk}^{(\ell)}\right), \qquad (36)$$

$$\begin{aligned}\tilde{Y}_n^{(\ell)} = {} & y_n^{(\ell)2} + 2y_n^{(\ell)}\left(y_n - y_n^{(\ell)}\right) - \frac{\Delta_n^{(\ell)2}}{v_0^2} \\ & + \frac{2}{v_0^2}(\mathbf{q}^{(\ell)}[n+1] - \mathbf{q}^{(\ell)}[n])^{\mathrm{T}} \qquad (37) \\ & \times (\mathbf{q}[n+1] - \mathbf{q}[n]),\end{aligned}$$

$$\tilde{R}_{nk}^{(\ell)} = R_{nk}^{(\ell)} + \nabla R_{nk}^{(\ell)\mathrm{T}}\left(\begin{bmatrix} u_{n1} - u_{n1}^{(\ell)} \\ \vdots \\ v_{nk} - v_{nk}^{(\ell)}\end{bmatrix}\right). \qquad (38)$$

The values $A_{nk}^{(\ell)}, y_n^{(\ell)}, \Delta_n^{(\ell)}, \mathbf{q}^{(\ell)}[n], u_{nw}^{(\ell)}, v_{nk}^{(\ell)}$, and $R_{nk}^{(\ell)}$ are the local points to obtain the lower bound, which are the results of the $(\ell-1)$-th iteration, and the gradient ∇R_{nk} can be calculated through the result of Appendix B. Note that, for the first iteration, we must define an initial case to compute the problem (P3). We will specify the initial case in Section 5.

Since the lower bounded constraints are all affine functions, the problem (P3) is now in the standard convex optimization problem form, thus, it can be solved effectively via problem solving tools such as CVX [34]. By iteratively solving the optimization problem and updating the local points, the solutions of (P3) will be in the feasible region of the original problem (P2), which converges to a KKT condition point. The proposed optimization technique is summarized in Algorithm 1. Note that, since the optimization problem is from the upper bound in (21), the resulting solution may not satisfy the data constraint in reality. To settle this issue, we can give a margin to the UE data constraint Q, e.g., $Q + \chi$ for some positive constant χ. Thus, by restraining the constraint, it will have a larger probability to satisfy the constraint in practice.

4.2 IRS Matching Case

While exploiting all the IRSs simultaneously might be the most straightforward method, it may not be the most probable solution. Considering that the IRS is a communication assisting object, the IRSs are likely to be located far apart. Hence, the power from the IRSs that are far apart from a UE is likely to be negligible. Also, the assumption that every IRS is controlled simultaneously for a single UE may be implausible. In result, the solutions from the general IRS usage case may be less practical.

Accordingly, we consider a more practical case that each UE is supported by only one IRS, where we denote it as the IRS matching case. The formulated optimization problem will effectively evaluate and decide which IRS to use per instance. The overall problem can be expressed as

$$\begin{aligned}(\text{P4}): \min_{\mathbf{T},\boldsymbol{\tau},\mathbf{q}} & \sum_{n=1}^{N}\left\{T_n P(V_n) + \sum_{k=1}^{K}\tau_{nk}P_c\right\} \\ \text{s.t. } & \sum_{n=1}^{N}\tau_{nk}\max_{w}\hat{R}_{nwk} \ge Q_k, \qquad \text{(P4-a)} \\ & \text{(P1-a), (P1-b), (P1-c),}\end{aligned}$$

where $\hat{R}_{nwk}$ represents the achievable rate of the k-th UE at the n-th segment when the UE is matched with the w-th IRS. Hence, with the maximum function in (P4-a), we pick the best IRS per instance for communication. Since we exploit only a single IRS, $\hat{R}_{nwk}$ is equivalent to (24) by considering the signals from only the w-th IRS, where we assume the signals from other IRSs are negligible. While we can still adopt the SCA technique due to the convexity of $\max_w \hat{R}_{nwk}$, the gradient is quite difficult to compute. Instead, we introduce a matching variable η_{nwk}, which represents the communication time between the k-th UE in the n-th segment using the w-th IRS. The overall problem

is given as

$$\text{(P5)}: \min_{\mathbf{T},\boldsymbol{\tau},\mathbf{q},\boldsymbol{\eta}} \sum_{n=1}^{N} \left\{ T_n P(V_n) + \sum_k \tau_{nk} P_c \right\}$$
$$\text{s.t.} \sum_{w=1}^{W} \eta_{nwk} \le \tau_{nk},\ \eta_{nwk} \ge 0, \qquad \text{(P5-a)}$$
$$\sum_{n,w} \eta_{nwk} \hat{R}_{nwk} \ge Q_k, \qquad \text{(P5-b)}$$
$$\text{(P1-a)}, \text{(P1-b)}, \text{(P1-c)},$$

where with the additional constraints (P5-a) and (P5-b), the solution will effectively force only one η_{nwk}, which is associated with the largest $\hat{R}_{nwk}$, to τ_{nk}, and the other $\eta_{nw'k}$ values to zero. By adopting the matching variable η_{nwk}, we successfully removed the maximum operation in (P4-a), and the gradient of $\hat{R}_{nwk}$ can be calculated through the results from the previous section since $\hat{R}_{nwk}$ has the same expression as (32) with a single IRS. As we can observe, by successfully transforming (P4) into (P5), (P5) is similar to (P1) with the additional linear constraint (P5-a), thus, we can solve the problem equivalently through the SCA technique. Note that, by choosing a single IRS for each instance, the IRS matching case can also resolve the rather strong assumption that the LoS paths between all the IRSs and UEs always exist, since the IRS closely located to a UE will have a high probability to have an LoS path. Accordingly, the IRS matching case is more practical than the general IRS usage case.

4.3 Low Complexity Algorithm

In this subsection, we propose a low complexity algorithm that attempts to follow the behavior of the optimized solutions described in the previous subsection. Through the simulation results in Section 5, we observe several factors. First, the IRS matching case has marginal performance loss than the general IRS usage case. Second, when the data constraint is small, the UAV directly goes to the final location with speed V_e, where V_e is the speed with the minimum energy consumption per meter, i.e., $V_e = \min_V P(V)/V$. Finally, when the data constraint is large, the UAV tends to communicate at fixed locations. To actively adapt to these characteristics, we introduce the following low complexity algorithm.

For this algorithm, we pair each UE with the closest IRS to mimic the IRS matching case, given the fact that the IRS matching case can suffice considerable performance. Before we specify the trajectory, we define several auxiliary variables. Through a one dimensional search between each UE and its paired IRS, we find the largest achievable rate location for each UE, denoted as $\hat{\mathbf{q}}_k$. Afterwards, we draw a straight line from $\mathbf{q}_0$ to $\mathbf{q}_F$, denoted as a toy trajectory. Next, we find the closest point from $\hat{\mathbf{q}}_k$ to the toy trajectory as $\bar{\mathbf{q}}_k$ by landing a vertical line on the toy trajectory from $\hat{\mathbf{q}}_k$. Using these variables, we will acquire the trajectory for the UAV.

Algorithm 2 Pseudo-code for the low complexity UAV energy consumption minimization algorithm

```
Pair each UE to its closest IRS
Find q̂_k and q̄_k.
Through the toy trajectory, find f.
if f_k ≥ 1, ∀k, then
    Set the toy trajectory as the solution.
else
    Compute (40).
    Solve the TSP of {q*_k} to find the shortest trajectory.
    Set the shortest trajectory as the solution.
end if
```

First, we simulate a toy scenario which follows the toy trajectory, moves with speed V_e, and performs equal time transmission for each UE at every segment, i.e., $\tau_{nk} = T_n/K$. From this toy scenario, we can compute the transmitted data as

$$\mathbf{r} = [f_1 Q_1, ..., f_K Q_K]^{\mathrm{T}}, \qquad (39)$$

where f_k is the fraction of data the UAV has transmitted with respect to the k-th UE with the data constraint Q_k. We can see that the fraction f_k indirectly implies the magnitude of the data constraint and distance between the toy trajectory and the UE, e.g., f_k will be small if Q_k is too large or the achievable rate is too small due to the large UE distance. Note that, if $f_k \ge 1,\ \forall k \in \{1, 2, ..., K\}$, we can simply select the toy scenario as the algorithm solution. Otherwise, we fix the transmit locations as

$$\mathbf{q}_k^\star = \hat{\mathbf{q}}_k + g_k(\mathbf{f}) \left(\bar{\mathbf{q}}_k - \hat{\mathbf{q}}_k \right), \qquad (40)$$

where $\mathbf{q}_k^\star$ denotes the transmit location for the k-th UE, $\mathbf{f} = [f_1, ..., f_K]^{\mathrm{T}}$, and $g_k(\mathbf{f})$ is a well defined function to choose the internal division point between $\bar{\mathbf{q}}_k$ and $\hat{\mathbf{q}}_k$ using $\mathbf{f}$. With the transmit locations $\{\mathbf{q}_k^\star\}$, we solve the traveling salesman problem (TSP) to find the shortest trajectory [15]. Finally, the UAV moves with the speed V_e and transmission takes place while the UAV is moving, and while the UAV is at the hovering locations. In specific, we first calculate the amount of transmitted data while the UAV is moving, and the remaining data is transmitted while hovering at the fixed locations $\{\mathbf{q}_k^\star\}$. In conclusion, the UAV will fly straight to $\mathbf{q}_F$ for small data constraints, and will fly to all the designated transmit locations $\{\mathbf{q}_k^\star\}$ in straight

lines for large data constraints. In this paper, we define $g_k(\mathbf{f}) = \min(f_k, 1)$. While determining the optimal $g_k(\mathbf{f})$ is itself another area of study, we consider it outside the scope of this paper. Nevertheless, the simple $g_k(\mathbf{f})$ is shown to have considerable performance in Section 5. The overall algorithm is summarized in Algorithm 2.

To confirm the advantage of the low complexity algorithm, we derive the complexities of the proposed algorithms. For the low complexity algorithm, the complexity is bounded with the SNR computation from (25), which is given as $\mathcal{O}(KW^2N)$. Note that, the TSP algorithm is NP-hard, thus, the computational cost is dominant with the TSP as $\mathcal{O}(K^2 2^K)$ in theory. However, due to the small K compared to the other variables, and considering the fact that there are many efficient methods to compute the TSP algorithm, we neglect this factor.

For the general IRS usage and IRS matching cases that rely on the convex optimization problems, the complexity is generally intractable. However, we can derive a rough lower bound complexity of $\mathcal{O}(N^3(K + W)^3)$, which is the complexity of a linear programming case. Even with this loose lower bound, we observe that the complexity of the low complexity algorithm is minimal compared to the other two methods.

5 Results and Discussion

In this section, we verify and compare the performance of the proposed algorithms. For simulations, the altitude and heights are fixed as $H_{\mathrm{A}} = 100$ m, $H_{\mathrm{I}_w} = 20$ m, and $H_{\mathrm{U}_k} = 0$, and the number of IRS elements is fixed as $M_w = 500$. For the probabilistic LoS model, the parameters are fixed as $a_{\mathrm{U}_k} = 30$, $b_{\mathrm{U}_k} = 0.15$, $a_{\mathrm{I}_w} = 15$, $b_{\mathrm{I}_w} = 0.18$, $\theta_{\mathrm{U}_k} = 60°$, and $\theta_{\mathrm{I}_w} = 54.2°$. For the channel model, the coefficients are fixed as $\beta_0 = 10^{-4}$, $\alpha_{\mathrm{I}_w} = 2.2$, $\alpha_{\mathrm{U}_k} = 2.5$, $\alpha_{wk} = 3$, $\kappa_{\mathrm{I}_w} = 30$, $\kappa_{\mathrm{U}_k} = 20$, $\kappa_{wk} = 10$, $\sigma^2 = -174$ dBm, and $B = 1$ MHz. For the communication scenario, the parameters are fixed as $\mathbf{q}_0 = [0, 0]^{\mathrm{T}}$, $\mathbf{q}_{\mathrm{F}} = [100, 100]^{\mathrm{T}}$, $\Delta_{\max} = 1$ m, $V_e = 18.3$ m/s, $V_{\max} = 30$ m/s, $N = 150$, and we assume that Q_k is the same for all UEs for simplicity. We construct a simple solution, i.e., hover and transmit at the UE locations, and use it for the initial case for the algorithms adopting the SCA technique. In the figures, the UEs are denoted as black circles and the IRSs are denoted as black diamonds.

Additionally, we adopt two benchmarks. First, the no IRS case by setting $p_{\mathrm{I}_w} = 0$, denoted as 'No IRS.' Second, we adopt the proposed algorithm in [31] as another benchmark, where it maximizes the average reception power. Note that, for fairness, we set the time constraint in [31] so that the data constraint is satisfied.

In Fig. 3, we plot the UAV energy consumption with respect to the number of iterations. The general IRS usage case and IRS matching case are denoted as 'General' and 'IRS matching', respectively. We observe that the proposed algorithms are non-decreasing with the number of iterations. Thus, we confirm that the proposed algorithms are indeed well manufactured through the SCA technique.

In Fig. 4, we observe the UAV trajectory for the IRS matching case with different data constraints. The figure shows that the UAV trajectory follows a straight line for a small data constraints, and steadily shifts towards the UE locations as the data constraint increases. These results follow our intuition. When the data constraint is small, the UAV can easily satisfy the data constraint from a far distance, so it uses the minimum flight power by simply flying on a straight line. As the data constraint increases, the UAV must find a balance between the energy consumption due to flying and the increasing achievable rate from shorter distance between the UAV and UEs. Accordingly, as the rate constraint increases, there is an increasing need for high achievable rate, resulting in a trajectory shift towards the UEs. Note that, we observe some unnatural behavior in some of the trajectories such as loops. This phenomenon seems to occur due to the UAV power consumption model, i.e., the UAV power consumption is not minimized at $V = 0$, therefore; the UAV may need to keep moving near the UEs to reduce its power consumption unless the data constraint is too high. Note also that the solution of the optimization problem only converges to a local optimum since the problem is not in the standard convex optimization form.

In Figs. 5 and 6, we plot the UAV speed and UAV flight time with respect to the path discretization segment n for the IRS matching case with the scenario equivalent to Fig. 4. Note that the small data constraint cases have minimal flight time, which are all shown at the bottom of Fig. 6. We first observe that the UAV speed for the lowest data constraint case is a constant with V_e. This is expected, since, to reduce UAV energy consumption, the UAV must choose not only the shortest trajectory, but also the optimal speed for energy efficiency. Also, by jointly observing the speed and flight time, we find out that as the data constraint increases, the UAV has the tendency to slow down and communicate on a fixed location, which is the basis of our proposed low complexity algorithm.

In Fig. 7, we plot the trajectory of the UAV for the various techniques in two extreme data constraints. For the low data constraint, we observe that all the techniques converge to the same trajectory, confirming that the algorithms work in a consistent manner for the low data constraint. Also, it confirms that the

proposed low complexity algorithm adapts well to the low data constraint. For the high data constraint, we observe that the trajectories behave in a more involved manner, confirming that proper adjustment is needed for different communication requirements.

In Fig. 8, we plot the UAV energy consumption for different techniques with respect to the data constraint for the scenario equivalent to Fig. 7, which is denoted as $K = 2$, and the scenario with one UE and two IRSs closely located, denoted as $K = 1$. For both single UE and multiple UE scenarios, one UE has the two IRSs in close proximity, making it beneficial to the general IRS usage case. Since [31] only considers the single UE case, it is not simulated for the multiple UE scenario. The figure clearly shows that the proposed optimization problem solutions have outstanding performance with respect to the no IRS case, confirming that exploiting the IRS for UAV energy consumption minimization is a legitimate approach. The low complexity algorithm outperforms [31], showing that the UAV hovering power must be considered to achieve energy efficient UAV communication. The general IRS usage case works as a lower bound for any data constraint. This result is expected since the general IRS usage case exploits all the IRSs in the system, thus, will have the best performance. We also observe that the gap between the general IRS usage case and the IRS matching case becomes larger as the data constraint increases. This is due to the composition of the UAV energy consumption model. While for small data constraints, the UAV energy consumption is dominated by the flying power to the final location, which is inevitable. However, as the data constraint increases, the UAV hovers in a fixed location for communication, and the energy consumption from hovering for communication becomes dominant. Since the general IRS usage case will have the largest achievable rate, the energy consumption of hovering for communication will be generally smaller, resulting in better performance than the IRS matching case. Finally, we observe the performance of the proposed low complexity algorithm. In the low data constraint region, the low complexity algorithm has some performance loss due to the constant speed of the UAV. However, the low complexity algorithm has marginal performance loss with respect to the IRS matching case in the high data constraint region. We also have checked that the performance of the low complexity case converges to the IRS matching case with a extremely high data constraint, which confirms that the proposed low complexity algorithm works sufficiently well in the high data constraint region with a simply defined $g_k(\mathbf{f})$. The low complexity algorithm can be further improved by optimizing the speed of UAV for the low data constraint region, which is an interesting future research topic.

6 Conclusion

In this paper, we proposed several techniques to minimize the UAV energy consumption in a general multiple IRS multiple UE scenario. We successfully incorporated the probabilistic LoS model to ensure the advantages of highly located IRSs. Through some approximations, we transformed and derived the problem of interest into a tractable form, which could be solved by the SCA technique. Employing various approaches, we derived the general IRS usage case that exploits all the IRSs simultaneously and the IRS matching case that actively selects the best IRS for transmission. We also proposed the low complexity algorithm that mimics the behavior of IRS matching case. By comparing with benchmarks, we confirmed that exploiting the IRSs in UAV communication systems is indeed favorable to minimize the UAV energy consumption, and it is crucial to consider the UAV hovering power for energy efficient UAV communication. In addition, we corroborated the fact that IRS matching techniques and simple trajectory planning may be sufficient in practice due to its marginal performance loss and with low complexity compared to the general IRS usage case.

Methods

This paper studies the energy consumption minimization of a UAV communication system with the aid of multiple intelligent reflecting surfaces. The performances of the proposed algorithms were evaluated by different settings and metrics. We use MATLAB R2021a to simulate the algorithms.

Appendix A
Proof of Lemma 1

Note that the functions

$$\log_2\left(\epsilon_z u_z^{-\alpha_z}\right) = -\alpha_z \log_2\left(u_z\right) + \log_2\left(\epsilon_z\right), \tag{41}$$

$$\log_2\left(\zeta_z\zeta_i u_z^{-\alpha_z/2} u_i^{-\alpha_i/2}\right) = -\frac{\alpha_z}{2}\log_2\left(u_z\right) - \frac{\alpha_i}{2}\log_2\left(u_i\right) + \log_2\left(\zeta_z\right) + \log_2\left(\zeta_i\right), \tag{42}$$

are convex with respect to u_z and u_i, since the logarithmic function is concave and $\alpha_z \geq 0$. Accordingly, the functions $\epsilon_z u_z^{-\alpha_z}$ and $\zeta_z\zeta_i u_z^{-\alpha_z/2} u_i^{-\alpha_i/2}$ are log-convex functions. With the same approach, we can also find out that a constant value is also a log-convex function.

By exploiting the fact that the sum of log-convex functions is log-convex, we see that the function $f(u_1, ..., u_Z)$ is the sum of log-convex functions, which finishes the proof.

Appendix B

For the function

$$f(u_1, ..., u_Z) = \log_2 \left(h(u_1, ..., u_Z) \right), \tag{43}$$

the derivative with respect to u_z is given as

$$\frac{df}{du_z} = \frac{-\alpha_z \epsilon_z u_z^{-\alpha_z - 1} - \sum_{i \neq z}^{Z} -\alpha_z \zeta_z \zeta_i u_z^{-\alpha_z/2 - 1} u_i^{-\alpha_i/2}}{h(u_1, ..., u_Z) \ln 2}. \tag{44}$$

In result, the derivative of $f(u_1, ..., u_Z)$ is expressed as

$$\nabla f = \left[\frac{df}{du_1}, ..., \frac{df}{du_Z} \right]^{\mathrm{T}}. \tag{45}$$

Abbreviation

UAV: Unmanned aerial vehicle; BS: Base station; IRS: Intelligent reflecting surface; LoS: Line-of-sight; UE: User equipment; SCA: Successive convex approximation; TDMA: Time-division multiple access; CSI: Channel state information; SNR: Signal-to-noise ratio; KKT: Karush-Kuhn-Tucker; TSP: Traveling salesman problem.

Acknowledgements

The authors thank S. Kang and B. Ko at KAIST for helping with the derivation of Appendix A and designing Fig. 1, respectively.

Availability of data and materials

The datasets used and/or analysed during the current study are available from the corresponding author on reasonable request.

Author's contributions

All authors read and approved the final manuscript.

Competing interests

The authors declare that they have no competing interests.

References

1. Xiao, Z., Xia, P., Xia, X.: Enabling UAV Cellular With Millimeter-Wave Communication: Potentials and Approaches. IEEE Communications Magazine **54**(5), 66–73 (2016)
2. Zeng, Y., Zhang, R., Lim, T.J.: Wireless Communications With Unmanned Aerial Vehicles: Opportunities and Challenges. IEEE Communications Magazine **54**(5), 36–42 (2016)
3. de Freitas, E.P., Heimfarth, T., Netto, I.F., Lino, C.E., Pereira, C.E., Ferreira, A.M., Wagner, F.R., Larsson, T.: UAV Relay Network to Support WSN Connectivity. International Congress on Ultra Modern Telecommunications and Control Systems, 309–314 (2010)
4. Ji, B., Li, Y., Zhou, B., Li, C., Song, K., Wen, H.: Performance Analysis of UAV Relay Assisted IoT Communication Network Enhanced With Energy Harvesting. IEEE Access **7**, 38738–38747 (2019)
5. Li, B., Fei, Z., Zhang, Y., Guizani, M.: Secure UAV Communication Networks over 5G. IEEE Wireless Communications **26**(5), 114–120 (2019)
6. Hu, X., Wong, K.-K., Yang, K., Zheng, Z.: UAV-Assisted Relaying and Edge Computing: Scheduling and Trajectory Optimization. IEEE Transactions on Wireless Communications **18**(10), 4738–4752 (2019)
7. Naqvi, S., Chakareski, J., Mastronarde, N., Xu, J., Afghah, F., Razi, A.: Energy Efficiency Analysis of UAV-Assisted mmWave HetNets, 1–6 (2018)
8. Chakareski, J., Naqvi, S., Mastronarde, N., Xu, J., Afghah, F., Razi, A.: An Energy Efficient Framework for UAV-Assisted Millimeter Wave 5G Heterogeneous Cellular Networks. IEEE Transactions on Green Communications and Networking **3**(1), 37–44 (2019)
9. Alzenad, M., El-Keyi, A., Lagum, F., Yanikomeroglu, H.: 3-D Placement of an Unmanned Aerial Vehicle Base Station (UAV-BS) for Energy-Efficient Maximal Coverage. IEEE Wireless Communications Letters **6**(4), 434–437 (2017)
10. Saxena, V., Jaldén, J., Klessig, H.: Optimal UAV Base Station Trajectories Using Flow-Level Models for Reinforcement Learning. IEEE Transactions on Cognitive Communications and Networking **5**(4), 1101–1112 (2019)
11. Zhang, S., Zhang, H., He, Q., Bian, K., Song, L.: Joint Trajectory and Power Optimization for UAV Relay Networks. IEEE Communications Letters **22**(1), 161–164 (2018)
12. Chen, X., Hu, X., Zhu, Q., Zhong, W., Chen, B.: Channel Modeling and Performance Analysis for UAV Relay Systems. China Communications **15**(12), 89–97 (2018)
13. Zeng, Y., Wu, Q., Zhang, R.: Accessing From the Sky: A Tutorial on UAV Communications for 5G and Beyond. Proceedings of the IEEE **107**(12), 2327–2375 (2019)
14. Zeng, Y., Zhang, R.: Energy-Efficient UAV Communication With Trajectory Optimization. IEEE Transactions on Wireless Communications **16**(6), 3747–3760 (2017)
15. Zeng, Y., Xu, J., Zhang, R.: Energy Minimization for Wireless Communication With Rotary-Wing UAV. IEEE Transactions on Wireless Communications **18**(4), 2329–2345 (2019)
16. Saad, W., Bennis, M., Chen, M.: A Vision of 6G Wireless Systems: Applications, Trends, Technologies, and Open Research Problems. IEEE Network **34**(3), 134–142 (2020)
17. Björnson, E., Sanguinetti, L., Wymeersch, H., Hoydis, J., Marzetta, T.L.: Massive MIMO is a Reality—What is Next?: Five Promising Research Directions for Antenna Arrays. Digital Signal Processing **94**, 3–20 (2019)
18. Cho, H., Choi, J.: Alternating Beamforming With Intelligent Reflecting Surface Element Allocation. IEEE Wireless Communications Letters **10**(6), 1232–1236 (2021)
19. Renzo, M.D., Debbah, M., PhanHuy, D.: Smart Radio Environments Empowered by Reconfigurable AI Meta-Surfaces: An idea whose time has come. EURASIP Journal on Wireless Com Network (129) (2019)
20. Liaskos, C., Nie, S., Tsioliaridou, A., Pitsillides, A., Ioannidis, S., Akyildiz, I.: A New Wireless Communication Paradigm Through Software-Controlled Metasurfaces. IEEE Communications Magazine **56**(9), 162–169 (2018)
21. Basar, E., Renzo, M.D., Rosny, J.D., Debbah, M., Alouini, M., Zhang, R.: Wireless Communications Through Reconfigurable Intelligent Surfaces. IEEE Access **7**, 116753–116773 (2019)
22. Guo, H., Liang, Y., Chen, J., Larsson, E.G.: Weighted Sum-Rate Maximization for Reconfigurable Intelligent Surface Aided Wireless Networks. IEEE Transactions on Wireless Communications **19**(5), 3064–3076 (2020)
23. Li, S., Duo, B., Yuan, X., Liang, Y., Renzo, M.D.: Reconfigurable Intelligent Surface Assisted UAV Communication: Joint Trajectory Design and Passive Beamforming. IEEE Wireless Communications Letters **9**(5), 716–720 (2020)
24. Ma, D., Ding, M., Hassan, M.: Enhancing Cellular Communications for UAVs via Intelligent Reflective Surface. 2020 IEEE Wireless Communications and Networking Conference (WCNC), 1–6 (2020)
25. Wei, Z., Cai, Y., Sun, Z., Ng, D.W.K., Yuan, J., Zhou, M., Sun, L.: Sum-Rate Maximization for IRS-Assisted UAV OFDMA Communication Systems. IEEE Transactions on Wireless Communications **20**(4), 2530–2550 (2021)
26. Fang, S., Chen, G., Li, Y.: Joint Optimization for Secure Intelligent Reflecting Surface Assisted UAV Networks. IEEE Wireless Communications Letters **10**(2), 276–280 (2021)
27. Shafique, T., Tabassum, H., Hossain, E.: Optimization of Wireless Relaying With Flexible UAV-Borne Reflecting Surfaces. IEEE Transactions on Communications **69**(1), 309–325 (2021)
28. Yang, L., Meng, F., Zhang, J., Hasna, M.O., Renzo, M.D.: On the Performance of RIS-Assisted Dual-Hop UAV Communication Systems. IEEE Transactions on Vehicular Technology **69**(9), 10385–10390 (2020)
29. Mu, X., Liu, Y., Guo, L., Lin, J., Poor, H.V.: Intelligent Reflecting Surface Enhanced Multi-UAV NOMA Networks. IEEE Journal on Selected Areas in Communications **39**(10), 3051–3066 (2021)

30. Cai, Y., Wei, Z., Hu, S., Ng, D.W.K., Yuan, J.: Resource Allocation for Power-Efficient IRS-Assisted UAV Communications. 2020 IEEE International Conference on Communications Workshops (ICC Workshops), 1–7 (2020)
31. Ge, L., Dong, P., Zhang, H., Wang, J., You, X.: Joint Beamforming and Trajectory Optimization for Intelligent Reflecting Surfaces-Assisted UAV Communications. IEEE Access **8**, 78702–78712 (2020)
32. Al-Hourani, A., Kandeepan, S., Lardner, S.: Optimal LAP Altitude for Maximum Coverage. IEEE Wireless Communications Letters **3**(6), 569–572 (2014)
33. Sun, Y., Babu, P., Palomar, D.P.: Majorization-Minimization Algorithms in Signal Processing, Communications, and Machine Learning. IEEE Transactions on Signal Processing **65**(3), 794–816 (2017)
34. Grant, M., Boyd, S.: CVX: Matlab Software for Disciplined Convex Programming, version 2.1. `http://cvxr.com/cvx` (2014)

Figures

Figure 1: Single UAV downlink system with K UEs and W IRSs.

Figure 2: Achievable rate comparison among the approximated analytical values, the simulated results, and the bound from [15] for the single IRS single UE case. The UE is located at 250 m and the IRS is located at 245 m.

Figure 3: UAV energy consumption with respect to the number of iterations.

Figure 4: UAV trajectories for the IRS matching case for different data constraints.

Figure 5: UAV flight speed with respect to the path segment n for the IRS matching case with different data constraints.

Figure 6: UAV flight time with respect to the path segment n for the IRS matching case with different data constraints.

Figure 7: UAV trajectories in extreme data constraints.

Figure 8: UAV energy consumption with respect to the data constraint.

Figures

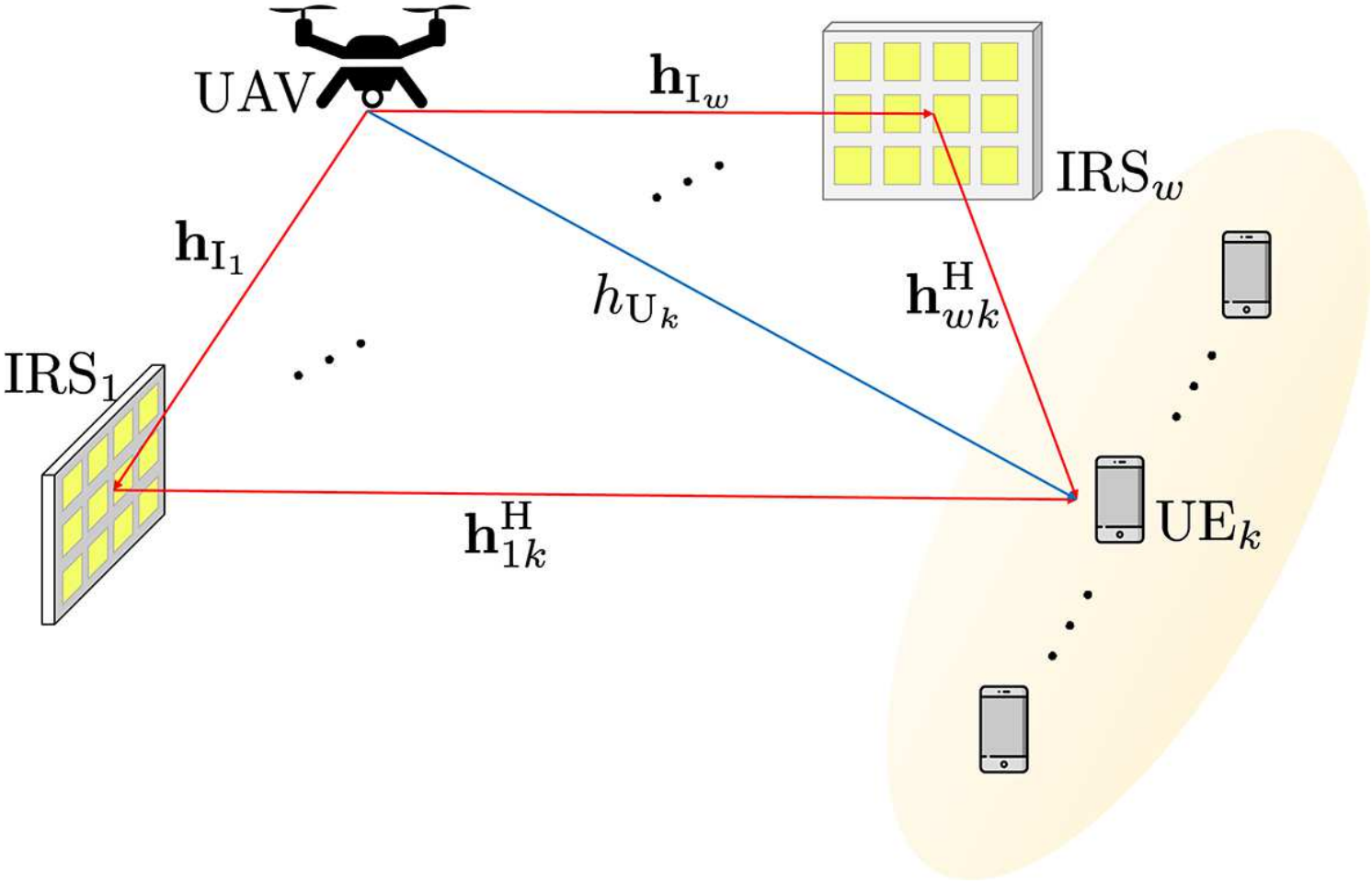

Figure 1

Single UAV downlink system with K UEs and W IRSs.

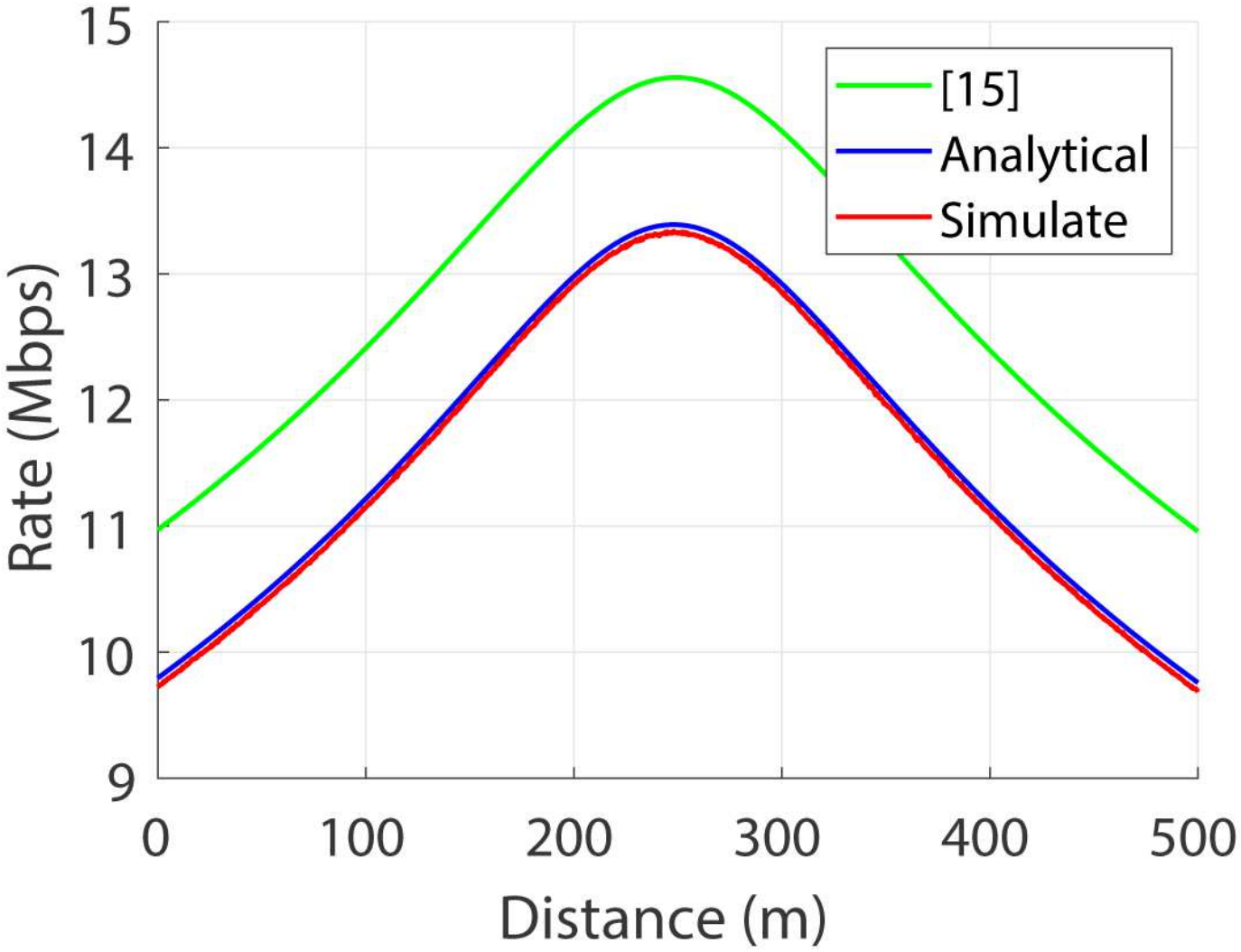

Figure 2

Achievable rate comparison among the approximated analytical values, the simulated results, and the bound from [15] for the single IRS single UE case. The UE is located at 250 m and the IRS is located at 245 m.

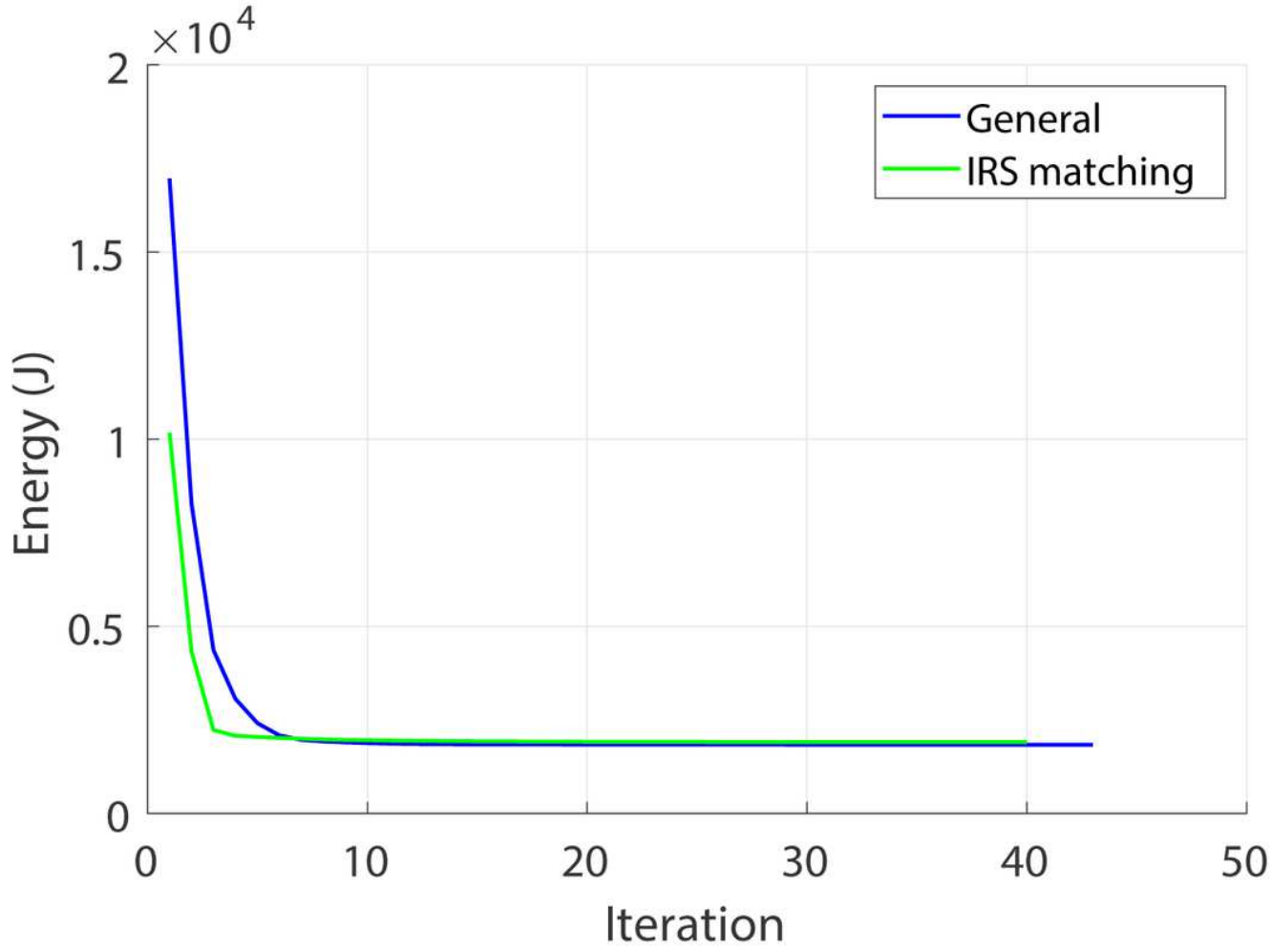

Figure 3

UAV energy consumption with respect to the number of iterations.

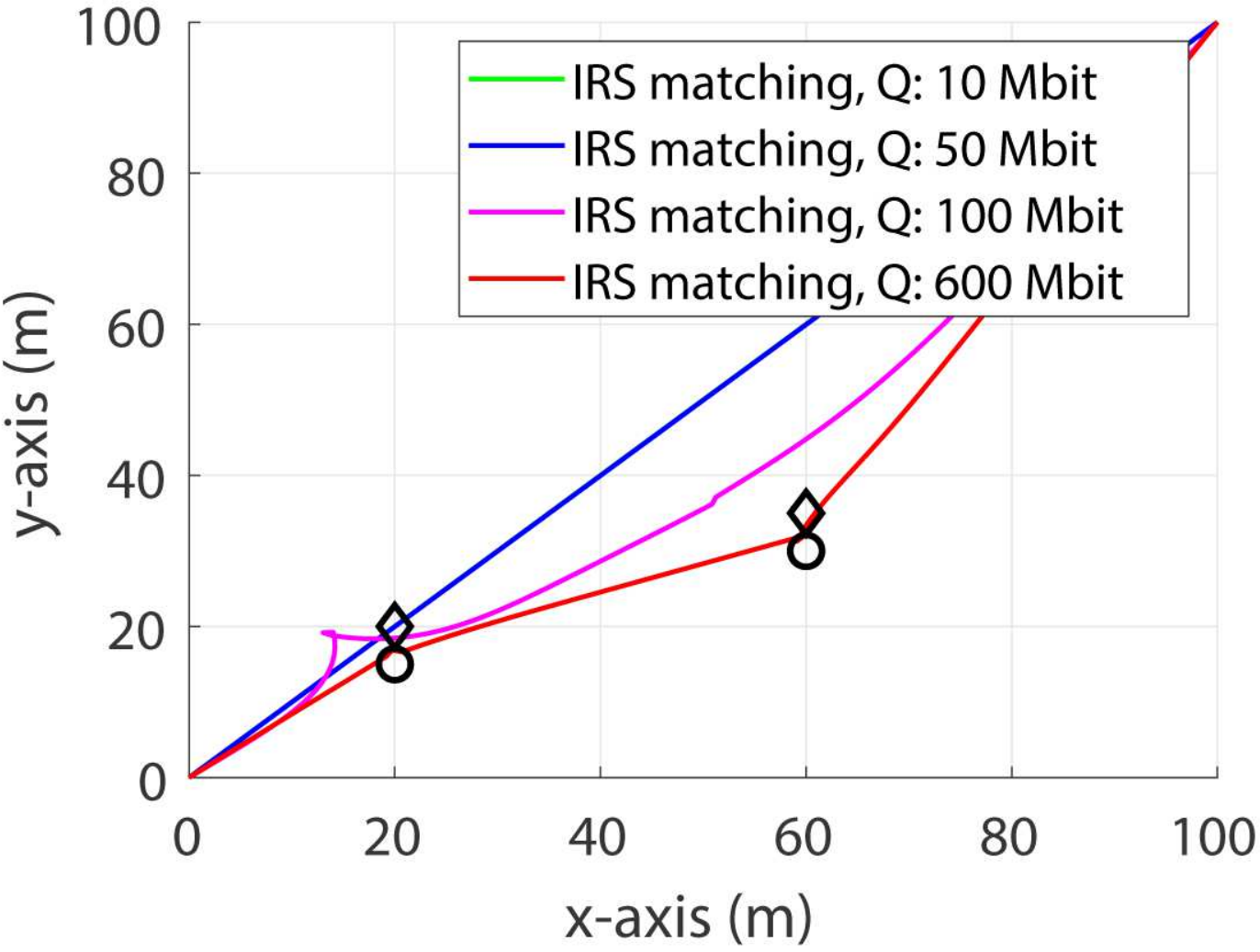

Figure 4

UAV trajectories for the IRS matching case for different data constraints.

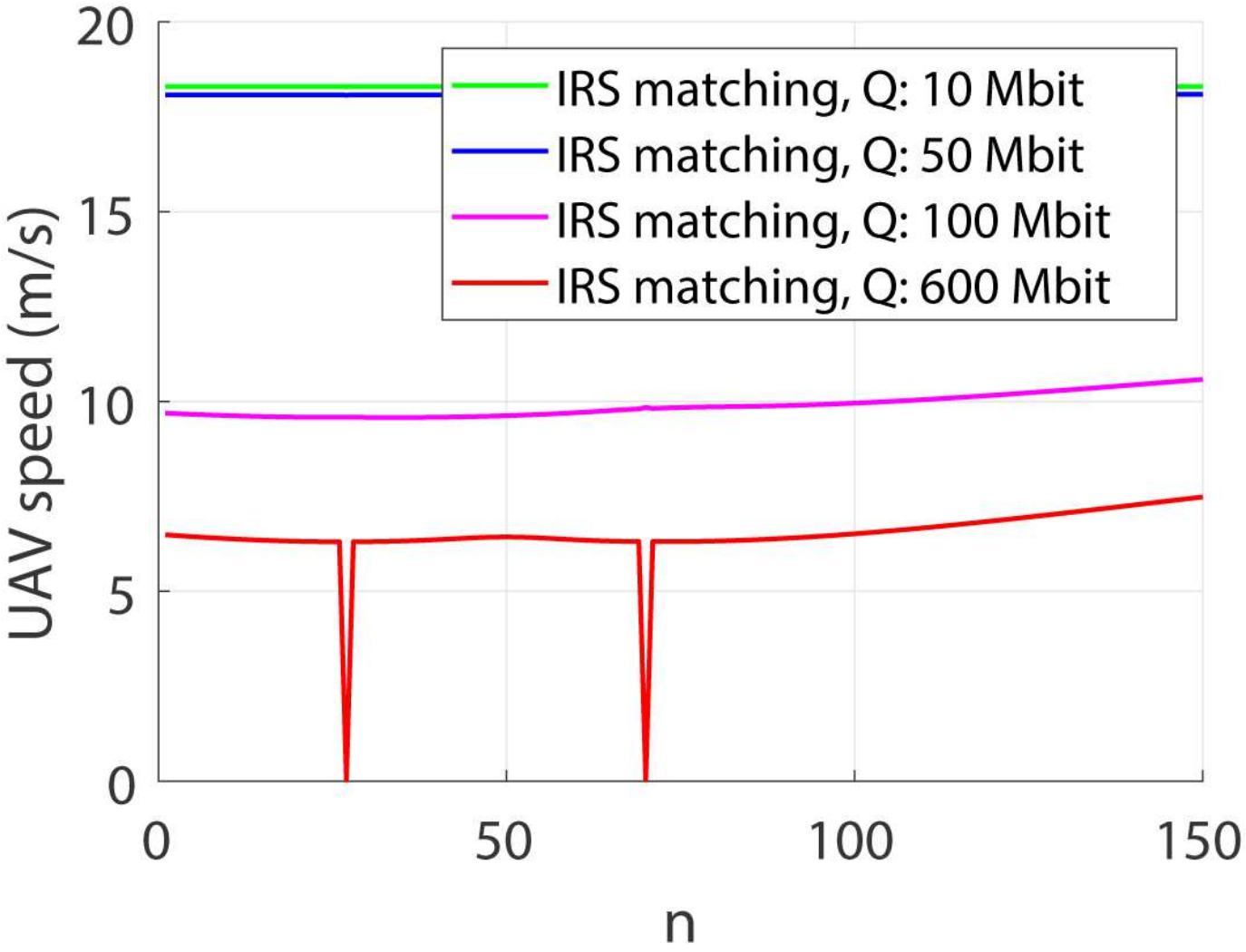

Figure 5

UAV ight speed with respect to the path segment n for the IRS matching case with different data constraints.

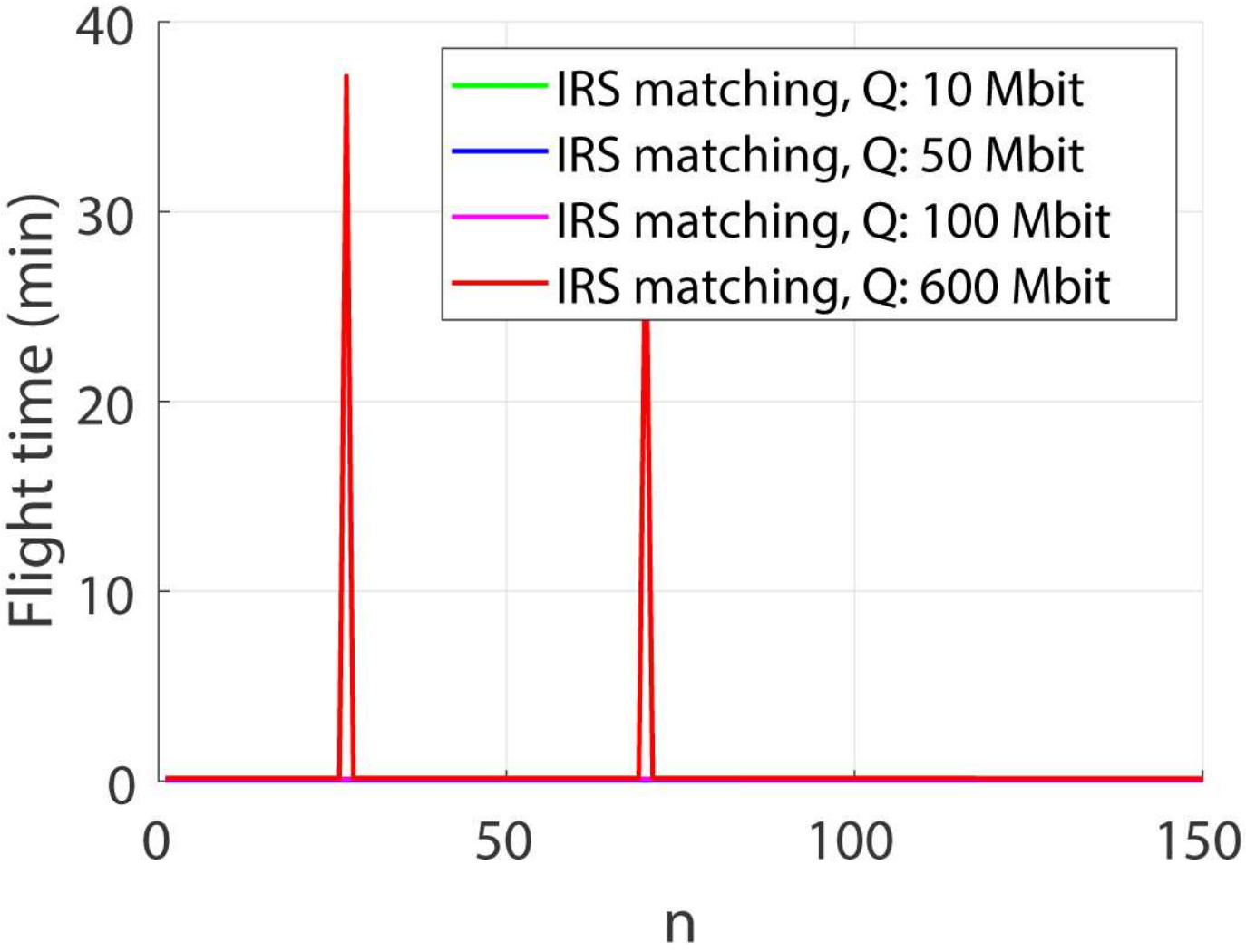

Figure 6

UAV ight time with respect to the path segment n for the IRS matching case with different data constraints.

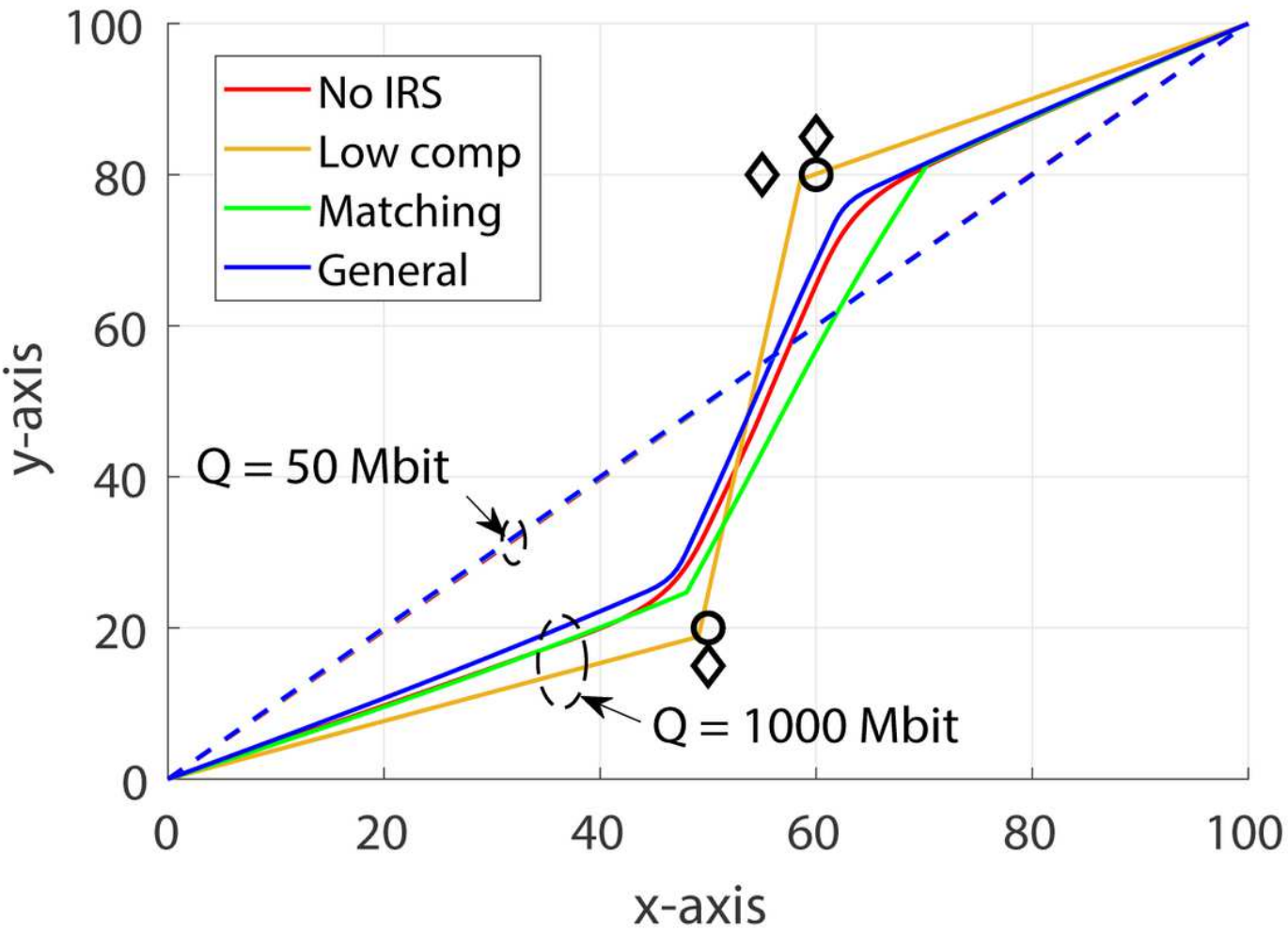

Figure 7

UAV trajectories in extreme data constraints.

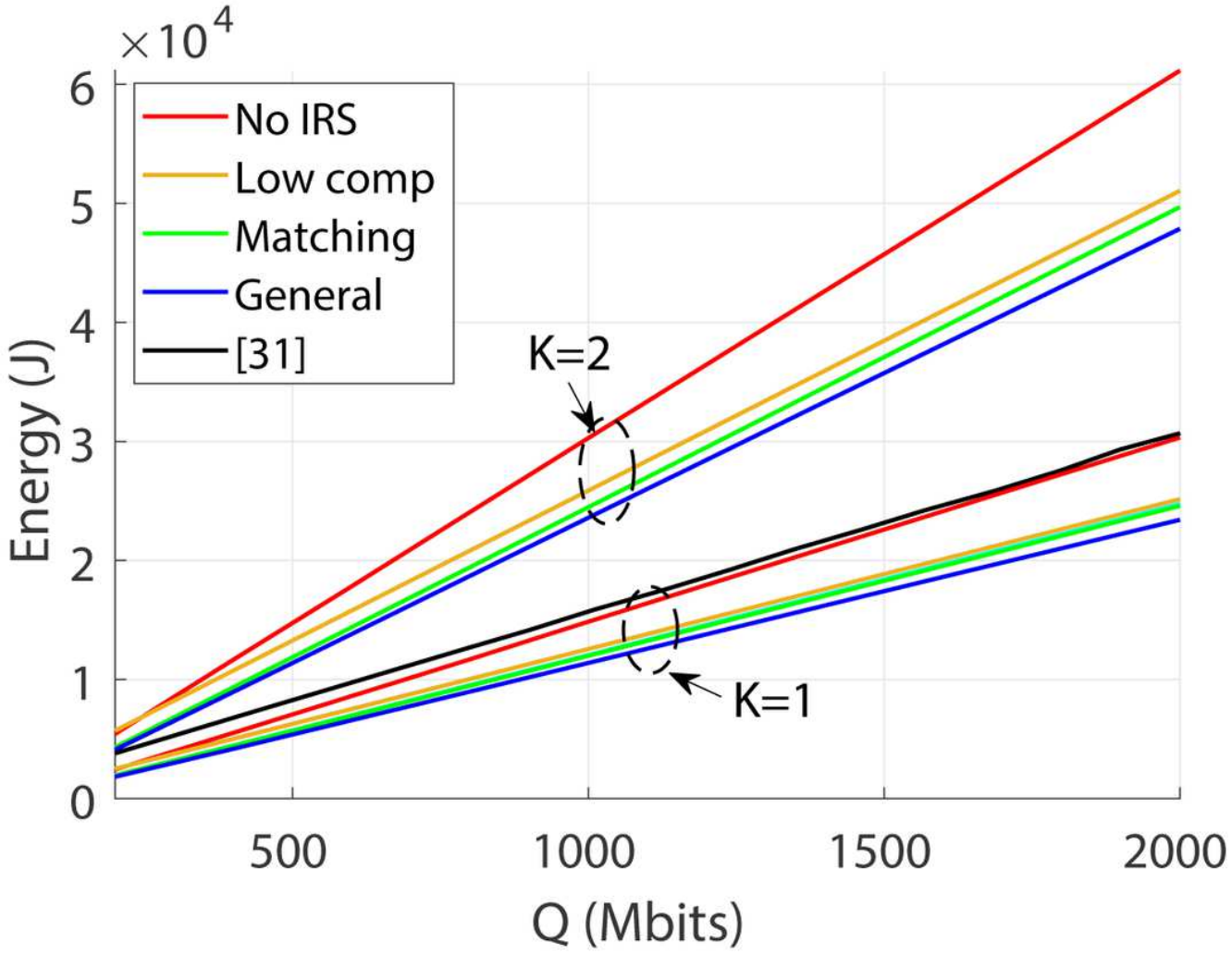

Figure 8

UAV energy consumption with respect to the data constraint.